Soft Matter

www.rsc.org/softmatter

Volume 8 | Number 7 | 21 February 2012 | Pages 2045–2330

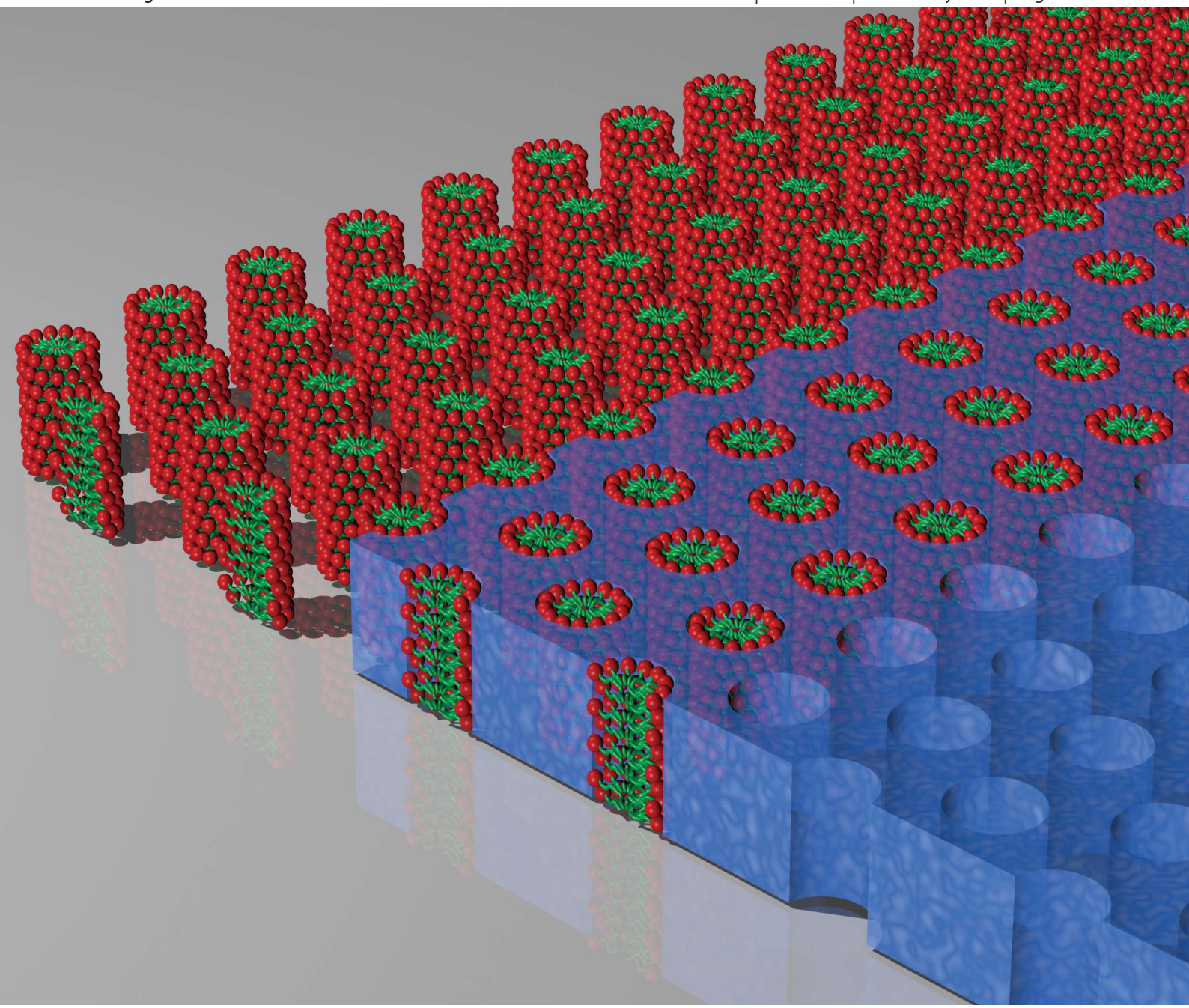

ISSN 1744-683X

RSC Publishing

PAPER

Lingxue Kong *et al.*

Structure retention in cross-linked poly(ethylene glycol) diacrylate hydrogel templated from a hexagonal lyotropic liquid crystal by controlling the surface tension

1744-683X(2012)8:7;1-G

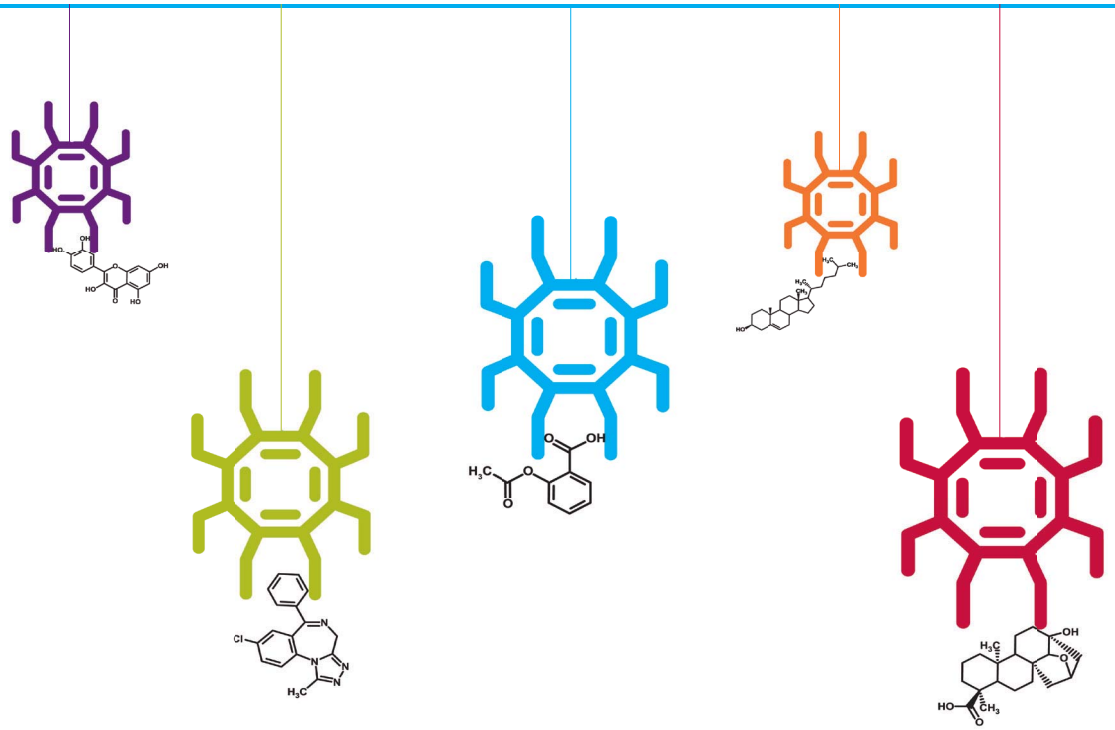

ChemSpider

The free chemical database

ChemSpider is a free chemical structure database providing fast access to over 25 million structures, properties and associated information. By integrating and linking compounds from more than 400 data sources, ChemSpider enables researchers to discover the most comprehensive view of freely available chemical data from a single online search.

Access ChemSpider anyplace, anytime, anywhere with the ChemSpider mobile website **http://cs.m.chemspider.com** or use the ChemSpider **mobile app** – just search for it on the apple app store and download it for free.

www.chemspider.com

Soft Matter

www.rsc.org/softmatter

RSC Publishing is a not-for-profit publisher and a division of the Royal Society of Chemistry. Any surplus made is used to support charitable activities aimed at advancing the chemical sciences. Full details are available from www.rsc.org

IN THIS ISSUE

ISSN 1744-683X CODEN SMOABF 8(7) 2045–2330 (2012)

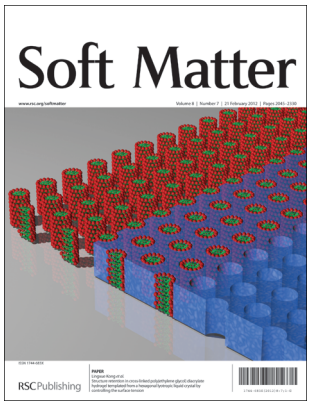

Cover

See Kong *et al.*, pp. 2087–2094.
Paolo Falcaro is acknowledged for assistance in creating the front-cover image.
Image reproduced by permission of Lingxue Kong from *Soft Matter*, 2012, **8**, 2087.

REVIEWS

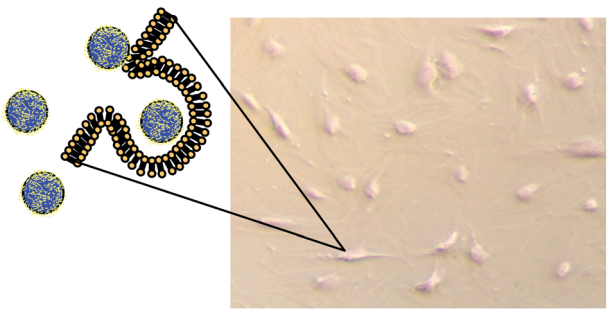

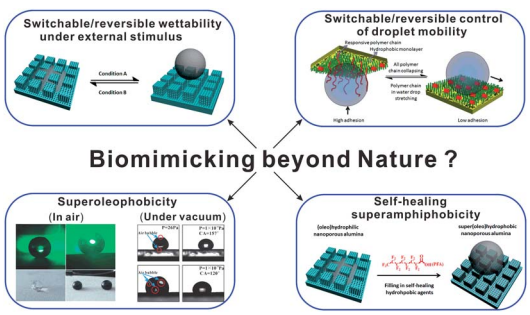

Soft Matter (print: ISSN 1744-683X; electronic: ISSN 1744-6848) is published 24 times a year by the Royal Society of Chemistry, Thomas Graham House, Science Park, Milton Road, Cambridge, UK CB4 0WF.

All orders, with cheques made payable to the Royal Society of Chemistry, should be sent to RSC Distribution Services, c/o Portland Customer Services, Commerce Way, Colchester, Essex, UK CO2 8HP. Tel +44 (0)1206 226050; E-mail sales@rscdistribution.org

2012 Annual (print+electronic) subscription price: £1,306; US$2,438. 2012 Annual (electronic) subscription price: £1,241; US$2,316. Customers in Canada will be subject to a surcharge to cover GST. Customers in the EU subscribing to the electronic version only will be charged VAT.

If you take an institutional subscription to any RSC journal you are entitled to free, site-wide web access to that journal. You can arrange access *via* Internet Protocol (IP) address at www.rsc.org/ip. Customers should make payments by cheque in sterling payable on a UK clearing bank or in US dollars payable on a US clearing bank. Periodicals postage paid at Rahway, NJ, USA and at additional mailing offices. Airfreight and mailing in the USA by Mercury Airfreight International Ltd., 365 Blair Road, Avenel, NJ 07001, USA.

US Postmaster: send address changes to Soft Matter, c/o Mercury Airfreight International Ltd., 365 Blair Road, Avenel, NJ 07001. All despatches outside the UK by Consolidated Airfreight.

Soft Matter

www.rsc.org/softmatter

Soft Matter is an international journal publishing high quality interdisciplinary fundamental research into all of soft matter, including complex fluids, with a particular focus on the interfaces between biology, physics, and chemistry, to include materials. The main research areas include: bulk soft matter assemblies, soft nanotechnology and self-assembly, biological aspects of soft matter, surfaces, interfaces, and interactions, building blocks/synthetic methodology, theory, modelling, and simulation.

INFORMATION FOR AUTHORS

Full details on how to submit material for publication in Soft Matter are given in the Instructions for Authors (available from http://www.rsc.org/authors). Submissions should be made *via* the journal's homepage: http://www.rsc.org/softmatter.

Submissions: The journal welcomes submissions of manuscripts for publication as Full Papers, Communications, Reviews, Tutorial Reviews, Emerging Areas, Highlights and Opinions. Full Papers and Communications should describe original work of high quality and impact.

Colour figures are reproduced free of charge where the use of colour is scientifically enhancing. Authors who wish to publish other figures in colour will be asked to contribute towards the costs of colour reproduction.
Additional details are available from the Editorial Office or http://www.rsc.org/authors

Authors may reproduce/republish portions of their published contribution without seeking permission from the RSC, provided that any such republication is accompanied by an acknowledgement in the form: (Original Citation)–Reproduced by permission of The Royal Society of Chemistry.

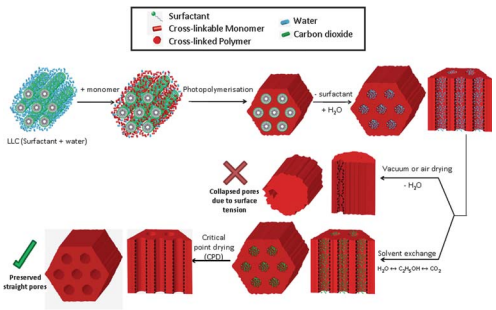

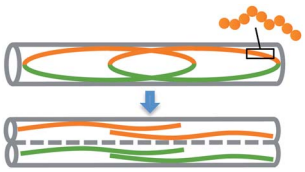

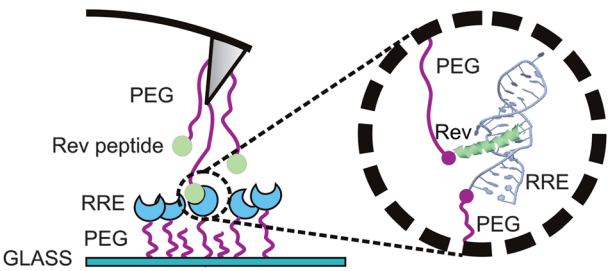

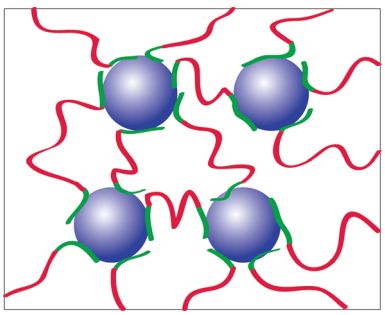

Affordable, high impact science

Free access to these journals is ending. You can continue to access high quality, high impact science through discounted packages or affordable institutional subscriptions.

Ask for a quote: sales@rsc.org

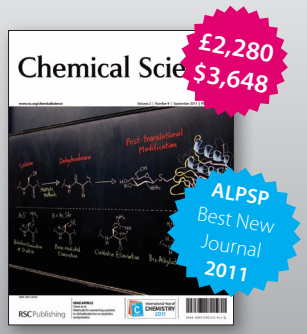

Buy online **www.rsc.org/buycs**

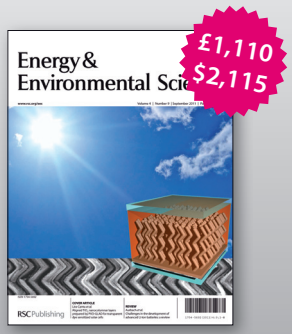

Buy online **www.rsc.org/buyees**

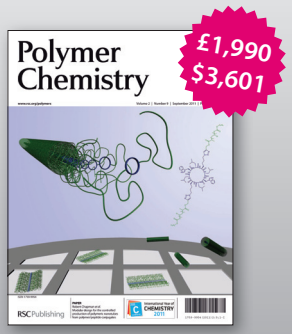

Buy online **www.rsc.org/buypc**

Buy online **www.rsc.org/buyfood**

Buy online **www.rsc.org/buymet**

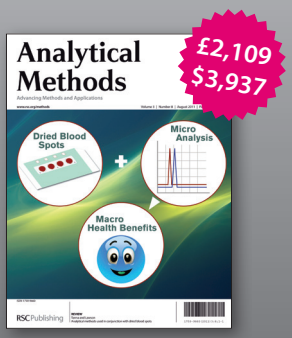

Buy online **www.rsc.org/buyam**

Buy online **www.rsc.org/buyib**

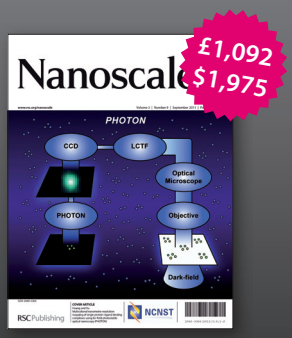

Buy online **www.rsc.org/buynano**

Buy online **www.rsc.org/buymed**

***online only price quoted**

RSC Publishing

www.rsc.org/publishing

Registered Charity Number 207890

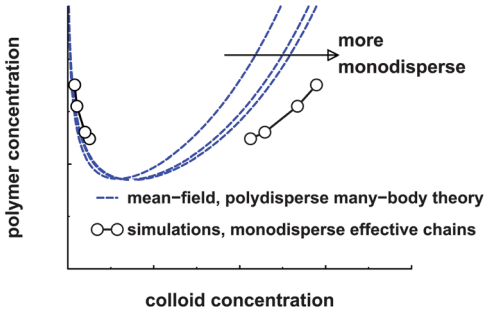

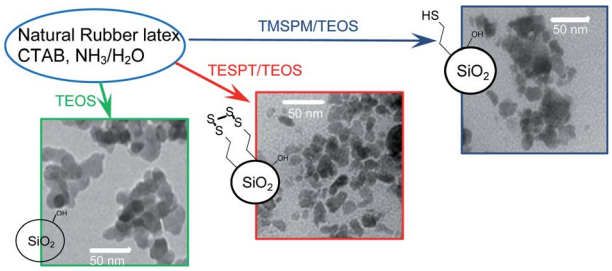

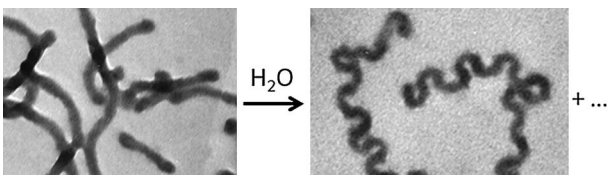

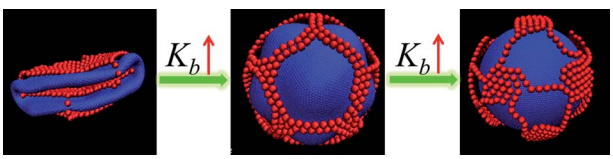

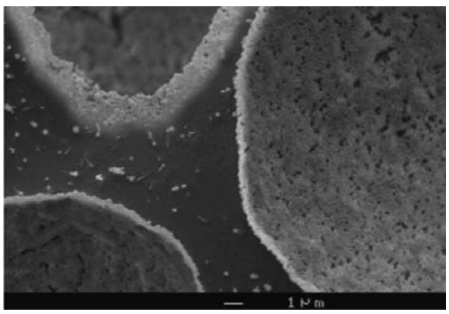

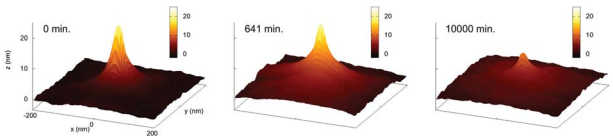

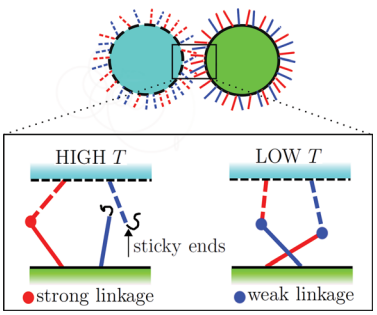

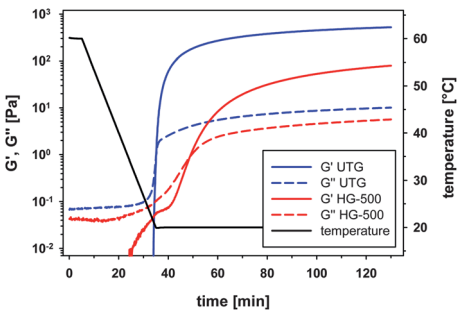

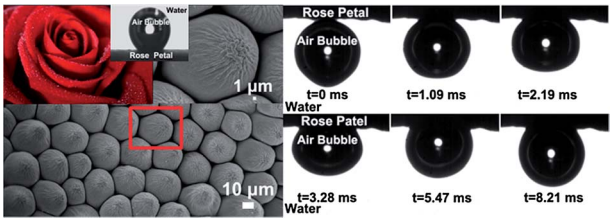

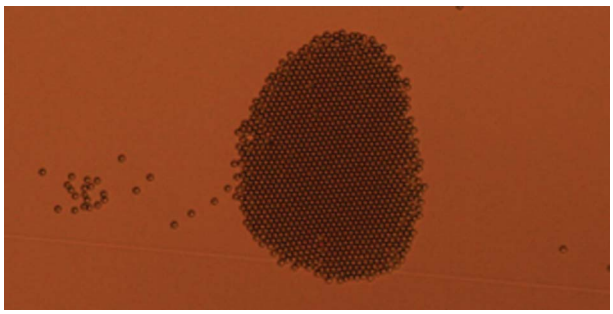

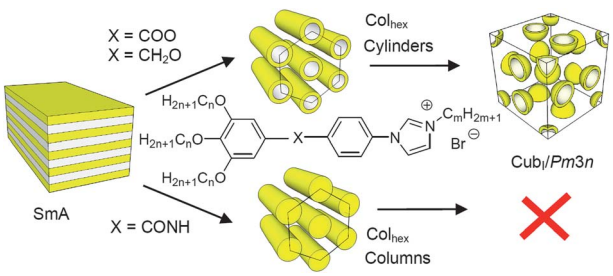

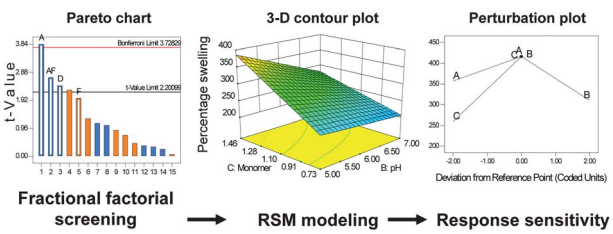

2294

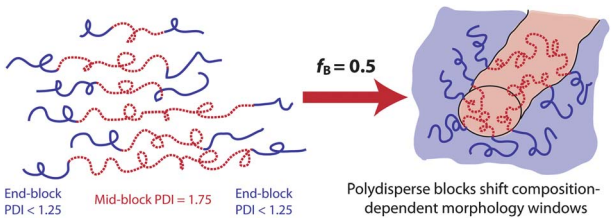

Polydispersity-driven shift in the lamellar mesophase composition window of PEO-PB-PEO triblock copolymers

Andrew L. Schmitt and Mahesh K. Mahanthappa*

Middle block polydispersity in OBO triblock copolymers shifts the lamellar morphology window, dilates the lamellar domains, and dramatically affects the observed equilibrium morphology.

2304

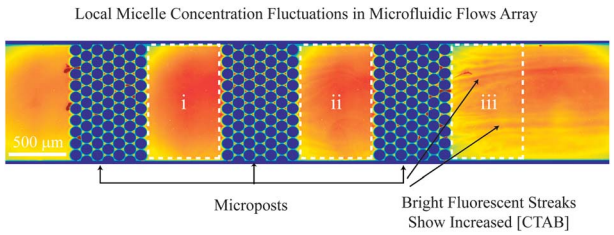

Local micelle concentration fluctuations in microfluidic flows and its relation to a flow-induced structured phase (FISP)

Perry Cheung, Neville Dubash and Amy Q. Shen*

Nile Red is used to monitor the local micelle concentration fluctuations of wormlike micelle solutions flowing in a microfluidic device. The flow-induced structured phase emerges at the higher concentration regions.

2310

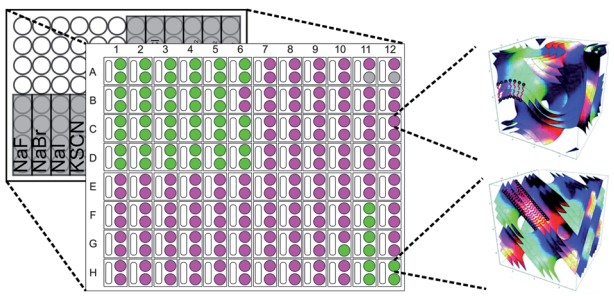

High-throughput analysis of the structural evolution of the monoolein cubic phase *in situ* under crystallogenesis conditions

Charlotte E. Conn,* Connie Darmanin, Xavier Mulet, Sophie Le Cann, Nigel Kirby and Calum J. Drummond

Structural evolution of the monoolein cubic phase under crystallogenesis conditions.

2322

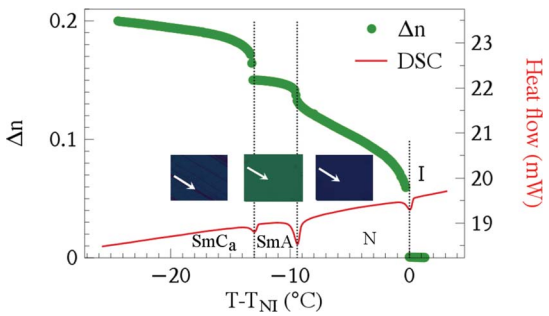

Structure–property correlation of a hockey stick-shaped compound exhibiting N-SmA-SmC$_a$ phase transitions

P. Sathyanarayana, S. Radhika, B. K. Sadashiva and Surajit Dhara*

Physical properties of a hockey stick-shaped compound are significantly different than calamitic compounds and partially similar to the bent-core compounds.

Soft Matter

Dynamic Article Links

Cite this: *Soft Matter*, 2012, **8**, 2261

www.rsc.org/softmatter

PAPER

Rose petals with a novel and steady air bubble pinning effect in aqueous media†

Jingming Wang,*[a] Qinglin Yang,[a] Mingchao Wang,[a] Chun Wang[a] and Lei Jiang[ab]

Received 9th September 2011, Accepted 23rd November 2011
DOI: 10.1039/c2sm06705f

Many well-known natural superhydrophobic surfaces exhibit unique characteristics when immersed in the aqueous medium. In the present paper, the phenomenon of the steady pinning effect of air bubbles on a rose petal with a combination of hierarchical rough structures (*i.e.*, micropapillae and nanofolds) is described. The pinning force of a 2 μL air bubble is *ca.* 101.2 μN, and the critical flow velocity of water leading the three-phase contact line (TPCL) to slide is as quick as 124.7 mm s^{-1}. The artificial rose petal surface was prepared from polydimethlsiloxane (PDMS) by a casting technique. It has the same nanofolds and micropapillae as the rose petal surface, and shows a similar air bubble pinning effect. The pinning force and the critical flow velocity of the artificial rose petal surface are 140.7 μN and 156.7 mm s^{-1}, respectively. Smooth and rough PDMS films with an ordered nanostructure or patterned microstructure are utilized to study the contribution of the micro/nano hierarchical structures to the air bubble pinning effect. Particularly, the facility that the captured air pockets in the nanostructure of the rose petals (*ca.* 500–600 nm in width on each micropapilla tip) coalesce with the air bubble is shown. The process where a periodic array of microstructures (diameter: 16 μm, height: 7 μm) construct "absorbed" islands to avoid the coalescence between the adjacent air pockets on the nanofolds is demonstrated as well. The important roles of the size and distribution of the microstructure of the rose petal in the air bubble pinning process are highlighted. This steady pinning effect induced on superhydrophobic surfaces with micro/nano hierarchical rough structures should spark further theoretical study on other bubble-related interfacial phenomena and should open a new avenue for their application in industrial processes, including the cleaning of boats contaminated by plankton and oil, reduction of drag friction on ships and submarine hulls, and the foaming control process.

1. Introduction

Many biological surfaces exhibit amazing characteristics, including the directional water collection on the backs of the desert beetle and wetted spider silk,[1] the dry-style antifogging effect of the compound-eyes of mosquitoes,[2] the effortless standing and quick waterborne movement of the legs of water spiders,[3] and the self-cleaning effect of lotus leaves.[4] Numerous studies have revealed that these interesting characteristics of the biological surfaces are attributed to their special wettabilities in combination with unusual micro/nano- hierarchical structures and chemical composition.[5] Inspired by nature, artificial surfaces with different wettabilities have been constructed and explored. These surfaces have immense importance in fundamental research and abundant potential applications.[6] However, research efforts have been devoted more to examine the surfaces with different wettabilities in air rather than in an aqueous medium.[7]

The wetting/dewetting properties of these surfaces have a number of equally important uses in the aqueous medium. These are crucial to the cleaning of boats contaminated by plankton and oil,[7] the reduction of drag friction on ships and submarine hulls,[8] and the foaming control process.[9] To carry out these processes, the surfaces must be ingeniously designed and the interaction between these surfaces and oil droplets/air bubbles in the aqueous medium (which involves two or more phases) should be completely understood. Fortunately, some aquatic organisms provide us representative examples and inspiration to design and create the above-mentioned interfacial materials. An intriguing example is the lotus leaf, which is famous for its self-cleaning effect in an air environment. It not only captures air to form an air protective layer to avoid being rusted in the aqueous medium, but also creates air bubbles

[a]*Key Laboratory of Bio-Inspired Smart Interfacial Science and Technology of Ministry of Education, School of Chemistry and Environment, Beihang University, 100191 Beijing, P. R. China. E-mail: wangjm@buaa.edu.cn; Fax: +86 10 8233 6066; Tel: +86 10 8233 6066*

[b]*Beijing National Laboratory for Molecular Sciences, Key Laboratory of Organic Solids, Institute of Chemistry, Chinese Academy of Sciences, 100190 Beijing, P. R. China. E-mail: jianglei@iccas.ac.cn; Fax: +86 10 8262 7566; Tel: +86 10 8262 1396*

† Electronic Supplementary Information (ESI) available: See DOI: 10.1039/c2sm06705f/

completely spread on its surface (*i.e.* so called air bubble bursting effect).[10] Therefore, it is believed that there are many well-known natural superhydrophobic surfaces that exhibit extraordinary characteristics when immersed in the aqueous medium.[7b] These will open a new avenue for applications in industrial processes.

In the present study, the behavior of an air bubble on the rose petal surface, a well-known natural superhydrophobic surface with high adhesive force for water droplets,[11] was investigated. Air bubbles showed the ability to pin themselves on the superhydrophobic rose petal. The pinning effect was maintained through strong pinning force because of the special hierarchical rough structures of the petal surface, which are composed of micropapillae and nanofolds. This effect was shown to be reproducible on an artificial rose petal, *i.e.*, a superhydrophobic polydimethylsiloxane (PDMS) film with similar hierarchical rough structures. Consequently, a plausible mechanism was proposed to explain the pinning effect in a three-phase system.

2. Experimental section

2.1. Superhydrophobic rose petals from nature

Fresh rose petals were obtained from a garden in Beijing, China. Samples of rose petals were cut into square pieces avoiding the veins. Each piece was *ca.* 10×10 mm^2 in size.

2.2. Fabrication of PDMS films with hierarchical structure inspired from rose petals, ordered nanostructure and patterned microstructure

The artificial petals were prepared by a casting technique. The micropapillae and nanofolds comprised the micro/nano hierarchical rough structures of the face of the rose petal surfaces, while the nanofolds constructed the back of the rose petal surfaces. Therefore, the face and back of the rose petal were use as the template to make PDMS films with hierarchical structure and nanofolds, respectively.[12] An aqueous solution of poly(vinyl alcohol) (PVA) (Mw $\approx$ 88 000 g mol^{-1}, *ca.* 10 wt%) was poured onto the front and back surfaces of a fresh rose petal and exposed to ambient conditions. When water evaporated completely at room temperature, the PVA films were peeled off; they contained the imprints of the inverse structures of the front and back of the rose petal surfaces. The PDMS films were subsequently obtained by pouring the precursor liquid mixed with the curing agent (10 : 1 w/w) onto the prepared PVA films, which were peeled off after curing the PDMS at 70 °C for *ca.* 2 h. The artificial rose petal and the PDMS film with nanofolds were consequently constructed. After the precursor liquid mixed with the curing agent (10 : 1 w/w) was pre-cured at 50 °C for 15–20 min, the PDMS films containing the patterned micropapillae with smooth surface were then obtained by pressing the precursor into the prepared PVA film with the inverse structure of the front petal surface. Subsequently, the film was peeled off after curing the PDMS at 70 °C for about 2 h. The patterned PDMS stamps were oxidized (30 s) in O_2 plasma to render the surface hydrophilic. The hydrophilic PDMS stamps were immersed in an ethanol solution (1.0 wt %) of hydrolyzed FAS-17 (Shin-Etsu Chemical Co., Ltd., Tokyo, Japan) for 10 h at room temperature and then dried under N_2.

2.3. Measurement

The surface structures of the rose petal and the patterned PVA or PDMS films were characterized using an environmental scanning electron microscope (ESEM) apparatus (Quanta FEG 250, Holland) under ESEM mode and low-vacuum mode, respectively. A square quartz cell ($25 \times 25 \times 30$ mm^3) filled with water was fixed into the Dataphysics OCA20 system (optical contact angle measurement), and the samples were positioned horizontally in the water at a depth of *ca.* 3 mm. All samples were immersed in the experimental apparatus for 30 min before testing to achieve a redistributed, well-proportioned air layer in water. Air bubbles were released from a bent needle (outer-Φ, 0.52 mm; inner-Φ, 0.26 mm; length, 57 mm; width, 15 mm; upward, 7 mm). Air bubbles could leave the needle orifice when the injection speed was greater than 10 μL s^{-1}. The volume of the exiting air bubble was *ca.* 2 μL and the distance between the sample surface and the needle orifice was fixed at *ca.* 3 mm. The bubble CA was measured by the captive bubble method (OCA20, Dataphysics Inc., Germany), and was used as a quantitative parameter to investigate air bubble behavior on different surfaces. The behavior of air bubbles on different surfaces was investigated by a high-speed camera (HCC1000F, VDS Vosskuhler GmbH, Germany) with a maximum rate of 1892 frames s^{-1}. Recording time was calculated by the frame frequency and number.

The force required to take the air bubble away from the substrate in the aqueous medium was measured using a high-sensitivity microelectromechanical balance system (Data Physics DCAT 11, Germany). The rose petal surface was placed in a square quartz cell ($25 \times 25 \times 30$ mm^3) filled with water, and the cell was fixed to the plate of the balance system. A 2 μL air bubble was suspended with a special metal ring, and the samples were placed on the balance table. The samples were moved upward at a constant speed of 0.01 mm s^{-1} until their surfaces contacted the air bubble. The force was increased gradually until it reached its maximum and the shape of the air bubble changed from spherical to elliptical. When the samples moved down further, the contact was sharply reduced to near zero and the shape of the air bubble changed back to spherical.

3. Results and discussions

3.1. Surface morphology and air bubble behavior on the rose petal

Fig. 1a illustrates the typical magnified ESEM image of a rose petal surface, wherein a periodic array of micropapillae with 16 μm average diameter and 7 μm height can be seen. The right inset of Fig. 1a shows of a papilla at higher resolution. The micropapilla exhibited nanosized cuticular folds *ca.* 500–600 nm in width at the tip. The micropapillae and the nanofolds comprised the micro/nano hierarchical rough structures of the rose petals surface. The surface is an example of a natural superhydrophobic surface with a high adhesive force for water droplets, *i.e.*, the so-called petal effect.[11,13] The air bubble pinning effect, which is similar to the petal effect, was observed on the rose petal surface when it was immersed in the aqueous medium. The air bubbles steadily pinned themselves to the petal surface even when the surface was turned upside down (left inset of Fig. 1a).

A high-speed camera was utilized to take a series of optical images. Fig. 1b shows clearly the dynamic pinning process of the

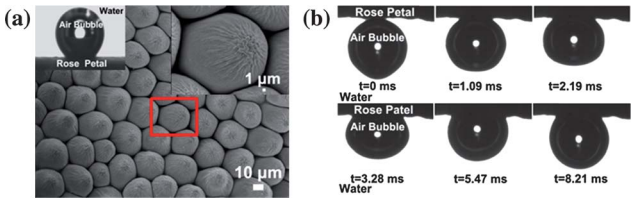

Fig. 1 ESEM images of the rose petal surface and optical images showing the air bubble pinning process. (a) ESEM images of a rose petal surface showing a periodic array of micropapillae and nanofolds on each papilla (right inset: a high-resolution image of a papilla; left inset: shape of an air bubble on the petal surface, indicating its air bubble pinning character when it is turned upside down). (b) A series of optical images showing the pinning process of a rising air bubble, at the time when the air bubble just contacted the rose petal surface before deformation was taken as the starting point, *i.e.*, $t = 0$.

air bubble. As the air bubble rose and at the first contact with the rose petal surface (*i.e.*, $t = 0$), it was nearly spherical. The contact area between air bubble and rose petal surface immediately expanded, while the shape of the air bubble changed slightly ($t =$ 1.09 ms). Subsequently, the air bubble spread out over the rose petal surface, and its shape started to change because of its buoyant force. After several microseconds a steady three-phase contact line (TPCL) formed, and the air bubble "pinned" itself to the rose petal surface ($t = 5.47$ ms). The final spherical shape of the air bubble was subsequently formed on the surface of the petal ($t = 8.21$ ms) and it was maintained thereafter. At this point, the bubble contact angle (CA) was 53.1°. Here, the bubble CA is the angle at which the liquid–air interface meets the solid–liquid interface. The bubble's CA is specific for any given system and is determined by the interactions of air bubble and the solid surfaces across the three interfaces. We defined this complete spreading-pinning process on the rose petal surface as the "air bubble pinning" effect.

In an air/water/solid system, the steadiness of the TPCL is crucial to the interactions between air bubbles and solid surfaces.[11,14] The movement of the TPCL was subsequently investigated when the volume of the air bubble increased and decreased (Fig. 2). The TPCL did not move at first when the volume of the air bubble increased. The air bubble TPCL started to move only when the increase in volume was large enough ($t =$ 1.59 s). From then on, the TPCL kept moving with the increase in the air bubble volume until the air bubble pinned itself to the rose petal surface again. Subsequently, the TPCL stopped moving despite the increase in the volume of the air bubble. The TPCL of the air bubble started to move again when its volume increased to a larger value ($t = 2.79$ s). The TPCL would repeat the "pinning-moving" cycle with the increase of the air bubble volume. However, the bubble CAs slightly changed during the whole process of the increase in air bubble volume. Furthermore, the decrease in the air bubble volume could be only observed instead of the movement of the TPCL, when air was continuously removed from the air bubble. That is, the TPCL was pinned when the air bubble volume decreased. However, for application in industrial processes, the steadiness of the TPCL of an air bubble in a flowing aqueous medium is more important than that in a still aqueous medium.[7b,15] Thus, the critical flow velocity of water, which can cause the TPCL of the air bubble slide, was measured using a flow control system (Fig. S1, ESI†). The results illustrated that the critical flow velocity of water that caused the TPCL of a 2 μL air bubble to slide was as high as 124.7 mm s^{-1}. This indicates a strong pinning action between air bubbles and the rose petal surface.

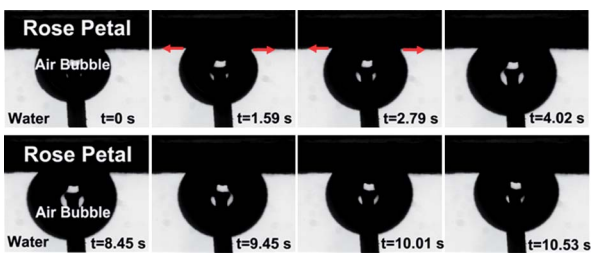

Fig. 2 A series of optical images showing the movement of TPCL when the volume of the air bubble increases and decreases on the rose petal surface.

Such strong pinning action can be assessed by a high-sensitivity microelectromechanical balance system.[7,16] An optical microscope lens and a charge-coupled device camera system were used to take photographs at the rate of one frame per second. Fig. 3 displays the recorded force–distance curves during the measuring process. A 2 μL air bubble was suspended on a metal ring in the water, and the force of this balance system was initially set to zero. Subsequently, the rose petal surface was brought into contact with the air bubble (Process 1). The rose petal surface moved at a rate of 0.01 mm s^{-1}. When the rose petal surface left the air bubble after contact, the balance force increased gradually and reached its maximum at the end of Process 2. Finally, the balance force decreased sharply when the rose petal surface broke away from the air bubble in Process 3, which ended the cycle of the force measurement. The force to which the air bubble was subjected can be regarded as the pinning force between the rose petal surface and the air bubble. The maximum force was approximately 101.2 μN at the point just before the air bubble left the petal surface. The final balance force did not return to zero because there was a little air left on the rose petal surface. Therefore, a slight increase of the force resulted from the decrease of the buoyancy of the air bubble.

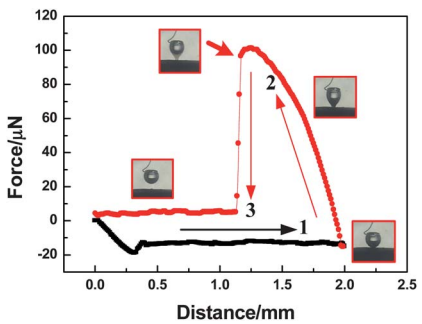

Fig. 3 Force–distance curves recorded before and after an air bubble contacted the rose petal surface. The inset shows four photographs of the shapes of the air bubble taken at the corresponding stages during the measurement process. Process1: the rose petal surface approached the air bubble; Process 2: the rose petal surface left the air bubble; Process 3: the rose petal surface broke away from the air bubble.

3.2. Surface morphology and air bubble behavior on the artificial rose petal

After viewing this novel phenomenon of the air bubble steady pinning effect of a rose petal surface, an artificial rose petal with similar micro/nano hierarchical structures was developed using the PDMS film. The behavior of air bubbles on this surface was investigated and the results are shown in Fig. 4. The ESEM images of the PVA films are shown in Fig. 4a. The PVA film had the inverse structures of the petal, with a close-packed array of approximately hemispherical concaves and ditches in the middle of the concave. Fig. 4b illustrates the representative ESEM images of the PDMS film, which was duplicated from the textured PVA film. Notably, the surface of the PDMS film with a periodic array of embossment showed remarkable microstructures and sizes which were the same as those in the original rose petal. Furthermore, the magnification of an artificial papilla (inset, Fig. 4b) reveals numerous nanofolds *ca.* 500–600 nm in width. The series of optical images in Fig. 4c were taken to study the behavior of the air bubble on the artificial rose petal surface. Air bubbles went through a similar pinning process as they did on the natural rose petal within 8.21 ms (bubble CA was 54.2°). The critical flow velocity of water, which caused the TPCL of the 2 μL air bubble to slide, was as quick as 156.7 mm s^{-1}. Furthermore, the pinning force of 2 μL air bubbles on the artificial rose petal was investigated. Fig. 4d displays the recorded force–distance curves during the measuring process. The maximum force was *ca.* 140.7 μN at the position just before the air bubble left the petal surface, which was larger than the force on rose petal surface.

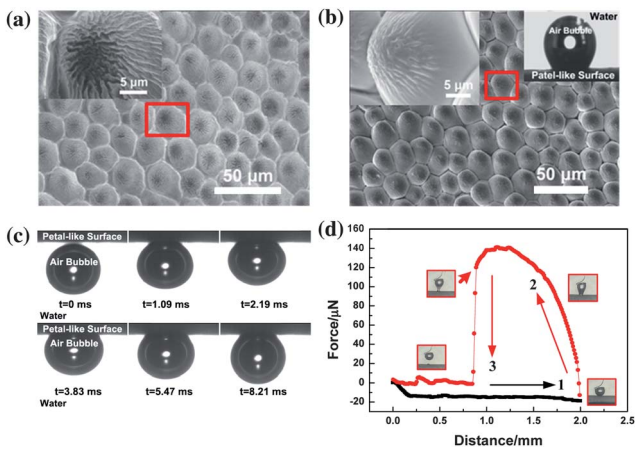

Fig. 4 ESEM images of the inverse and duplicated rose petal structures and the air bubble pinning effect on the artificial rose petal. (a) ESEM images of the duplicated PVA film with the inverse petal structure. (Inset: high-resolution image of the inverse petal structure). (b) ESEM images of the duplicated PDMS film with the similar surface structure of the petal. (Left inset: a high-resolution image of an artificial papilla with nanofolds; right inset: shape of air bubble on the surface of the artificial petal, indicating its air bubble pinning character when it is turned upside down). (c) A series of optical images showing the air bubble pinning process on the artificial rose petal surface. (d) Force–distance curves recorded before and after the air bubble contacted the artificial rose petal surfaces. The inset shows four photographs of the shapes of the air bubbles taken at the corresponding stages during the measurement process. Process1: the artificial rose petal surface approached the air bubble; Process 2: the artificial rose petal surface left the air bubble; Process 3: the artificial rose petal surface broke away from the air bubble.

3.3. Effect of micro/nano hierarchical rough structures on the air bubble pinning behavior

Micro/nano hierarchical rough structures always provide surfaces with a special wetting/dewetting effect.[5–7,17] Therefore, to confirm the importance of hierarchical rough structures on the air bubble pinning effect, the air bubble behaviors on hydrophobic smooth PDMS surfaces (average water CA of 102.7 ± 4.8°) were investigated, as shown in Fig. 5. When an air bubble collided with this smooth surface, it did not spread but bounced backward. The air bubble shape changed, and after several collision-bounce cycles, a steady TPCL finally formed, *i.e.*, the air bubble remained on the smooth surface (bubble CA of 67.5 ± 6.5°). This whole scenario took *ca.* 20 ms (Fig. 5a). Fig. 5b displays the recorded force–distance curves during the measuring process. The maximum force was *ca.* 26.5 μN at the point just before a 2 μL air bubble left the petal surface. These results indicated the importance of the hierarchical rough structures to the air bubble pinning effect.

To understand further the contribution of each scale rough structure on the air bubble pinning effect, PDMS films with ordered nanostructure or patterned microstructure were fabricated. ESEM images of a nanofold array and a micropapilla array are shown in Fig. 6a and b, respectively. The width of the nanofolds was about 500 nm (Fig. 6a). The bottom diameter and height of the micropapillae with smooth surfaces on the PDMS film were *ca.* 16 and 7 μm, respectively (Fig. 6b). Each series of optical images in Fig. 6a′ and b′ describes the air bubble behavior on the nanofold array and micropapilla array. When a rising air bubble contacted the nanofold array, the contact area between the air bubble and the nanofold array surface immediately expanded, and the air bubble shape changed until it had spread out over the nanofold array with a bubble CA of 134.5 ± 3.7°. In contrast, an air bubble spread slightly on the micropapilla array with bubble CA of 21.2 ± 4.5°. The force–distance curves of the nanofold array in Fig. 6a″ reveal that the interaction force between a 2 μL air bubble and the nanofolds was as strong as 225.4 μN, whereas the interaction force was as low as 8.9 μN (Fig. 6b″). These results demonstrate that the nanostructure played more roles in the pinning force of the rose petal than the microstructure did, while the microstructure avoided extensive spreading of the air bubble.

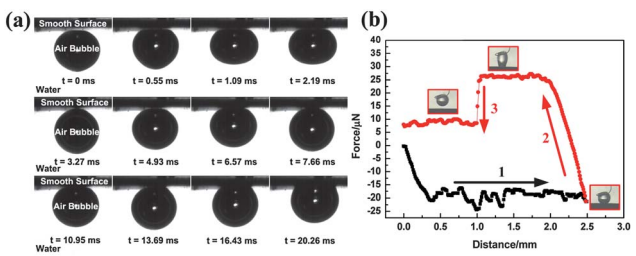

Fig. 5 Air bubble behavior on the smooth PDMS film. (a) A series of optical images showing air bubble behavior on the smooth PDMS film. (b) Force–distance curves recorded before and after the air bubble contacted the smooth PDMS film.

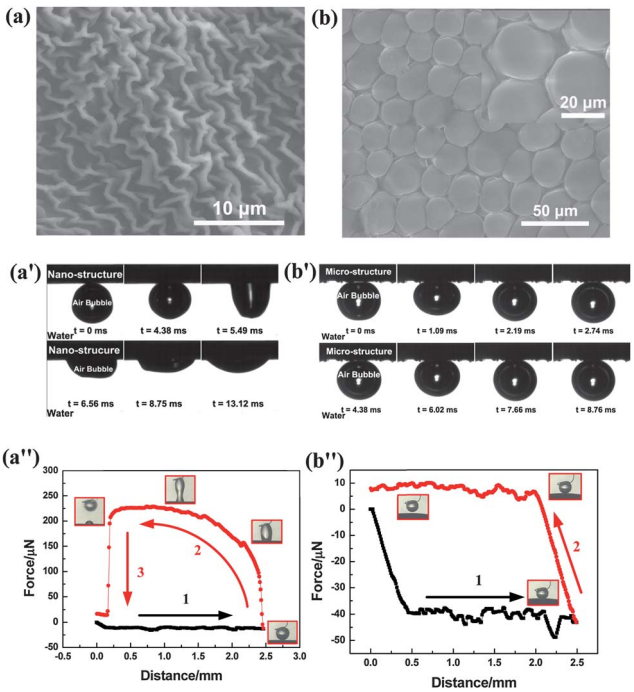

Fig. 6 ESEM images of the single-scale rough structure on PDMS films and the air bubble behaviors. (a) Top view of the large-area ordered nanofold array on the PDMS film. The width of nanofolds was *ca.* 500 nm. (a′) A series of optical images showing air bubble behavior on the nanofold array depicted in (a). (a″) Force–distance curves recorded before and after the air bubble contacted the nanofold arrays. (b) Top view of patterned micropapilla array. The bottom diameter and height of the micropapillae with the smooth surfaces were about *ca.* 16 and 7 μm, respectively. (b′) A series of optical images showing the air bubble pinning process on the micropapilla array in (b). (b″) Force–distance curves recorded before and after the air bubble contacted the micropapilla array.

The size of the micro/nano-hierachical structures is significant to the amazing characters of biological surfaces.[1b,2,10,11,18] Therefore, the influence of the rough structure size of the rose petal on the air bubble pinning effect was studied. The high elasticity PDMS film allowed it to be stretched to change the size of micro/nano-hierarchical structures.[19] The ESEM images of the stretched PDMS film reveal that the papillae distribution density per mm^2 decreased through stretching, (*i.e.*, both the bottom width and the spacing between the adjacent micropapillae increased), while the top width of the micropapillae and the structure of the nanofolds changed slightly (Fig. S2, ESI†). The interaction forces between air bubbles and the stretched PDMS film surface were investigated at different stretch ratios (Fig. 7). In this investigation, the stretch ratio is the variation of the PDMS film area before and after stretching. The interaction forces between a 2 μL air bubble and the PDMS film sharply decreased from 140 to 59 μN since the stretch ratio increased from 100% to 115%. Subsequently, the force decreased to 21 μN when the stretch ratio reached 130%. The interaction forces of a 2 μL air bubble could drop to 8 μN if the stretch ratio reached 145%, as shown by the blue bar in Fig. 7. Similarly, the interaction forces between a 5 μL air bubble and the PDMS film sharply decreased through stretching as well (from 280 μN).

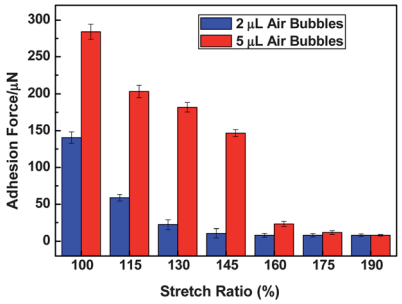

Fig. 7 Interaction forces between the PDMS film surface and air bubbles with two different volumes [(a) 2 μL; (b) 5 μL)] at different stretch ratio. The x-coordinate change from 100% to 190% represents the degree that the PDMS film surface was stretched.

The force dropped to 8 μN after the stretch ratio reached 190% (the red bar in Fig. 7). The papillae distribution density per mm^2 resulted in the reduction of the number of the active nanofolds on the micropapillae through the stretching of the PDMS film. Therefore, the nanostructure played a very important role in the pinning effect of the rose petal.

3.4. Characterization and analysis of the air bubble pinning effect

Theoretically, if the rose petal is immersed in the aqueous medium, the possibility of air trapping can be estimated by the threshold roughness r^*:[20]

$$r^* = 1 + \frac{\tan^2\theta_E}{4} \quad (1)$$

The formation of air pockets occurs if $\boldsymbol{r} > r^*$, where $\boldsymbol{r}$ is the ratio of the actual area of liquid–solid contact to the projected area on the horizontal plane, and $\boldsymbol{\theta_E}$ is the water contact angle of the smooth surface. According to the average size of nanofolds and micropapillae from the ESEM images of the rose petal, the calculated $\boldsymbol{r}$ of nanofolds and micropapillae were 7.87 and 1.32, respectively. (More details can be found in the ESI,† Fig. S4.) For $\boldsymbol{\theta_E} = 102°$ (the water CA of the smooth PDMS film is 102°), $\boldsymbol{r}^*$ is 6.53. the calculated results show that the water could enter into the micrpapillae of the petal but not into the nanofolds, and air pockets would be formed around the nanofolds. That is, the water film impregnates the texture; however, islands (air pockets) would always remain, and emerge above the absorbed water film.[11,17] As known, the water CA determined by the scale of roughness and chemical components is crucial to the state of the three phase contact interface. The higher the water CA, the greater the possibility of air pockets being trapped. Comparing the water CAs of the as prepared surfaces (Table S1, ESI† S3), the water CAs of the natural and artificial rose petal with hierarchical rough structures are the highest. Accordingly, the pinning force of the air bubble and the critical flow velocity of water leading the TPCL to slide are the largest.

Based on the experimental and calculated results above, a new mechanism was proposed to reveal the influence of the micro/nano hierarchical rough structures of the rose petal on the air bubble pinning effect, as shown in Fig. 8. Fig. 8a presents the schematic illustration of six micropapillae with nanofolds, which are immersed in water at a certain distance from the rising air

bubble. The thin water film that separates the solid surface from the air bubble is defined as the wetting film, and its stability is controlled by the interfacial interaction forces. Air pockets are captured around the nanofolds on each separate micropapilla. The wetting film gradually becomes thin as the rising air bubble approaches the rose petal surface. The attenuation of the wetting film finally leads to the coalescence of the air bubble with the air pockets around the nanofolds, resulting in the formation of fresh TPCLs. The wetting film around the air bubble keeps draining along the direction at the adjacent micropapillae shown by the arrows (Fig. 8b). The existing TPCLs move with the draining of the wetting film, and then other fresh TPCLs form (Fig. 8c). The existing TPCLs keep moving up and other fresh TPCLs continuously form until the air bubble has completely pinned itself (Fig. 8c and 8d).

4. Conclusion

In summary, a novel phenomenon of air bubble steady pinning on a rose petal surface at high pinning force and critical driving flow velocity was discovered. The underlying mechanism was attributed to the micro/nano hierarchical rough structures. Air pockets captured in the nanostructure of the rose petals easily coalesced with the air bubble, and the microstructure could form absorbed islands while avoiding the coalescence of adjacent air pockets around the nanofolds. Thus, the combination of nano- and microstructures was responsible for the air bubble pinning effect on the superhydrophobic surfaces. Moreover, the size and distribution of the microstructure of the rose petal played important roles in the air bubble pinning process. A superhydrophobic artificial rose petal, which mimicked the micro/nano hierarchical rough structures of the rose petal, was constructed. It showed a similar air bubble pinning effect. This steady pinning effect induced on superhydrophobic surfaces with micro/nano hierarchical rough structures should spark further theoretical studies on other bubble-related interfacial phenomena. From a practical standpoint, the findings have wide application in the bubble stabilization system, the cleaning of boats contaminated by plankton and oil, and the reduction of drag friction on ships and submarine hulls.

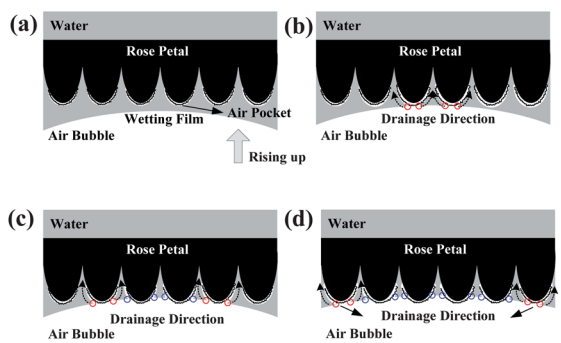

Fig. 8 Schematic model of the air bubble pinning process on the rose petal surface. (a) A rising air bubble approaching the rose petal surface. (b) The drainage of the wetting film around the air bubble along the direction shown by the arrows. The fresh TPCLs are formed (in the red circles). (c) The wetting film around the air bubble keeps draining along the direction at the adjacent rose petals shown by the arrows. The existing TPCLs move (in the blue circles) and other fresh TPCLs are formed. (d) The process of the fresh TPCLs forming. Here, the TPCL is the gas/liquid/solid interfaces in the red/blue circles, the cross-section view of which is shown by two points.

Acknowledgements

This work was supported by a grant from the National Nature Science Foundation of China (20901006), and the Innovation Foundation of the Chinese Academy of Sciences for continuing financial support. Also, thanks to Dr Yizhuo Gu for helpful discussions and suggestions.

Notes and references

1 (*a*) A. R. Parker and C. R. Lawrence, *Nature*, 2001, **414**, 33; (*b*) Y. Zheng, H. Bai, Z. Huang, X. Tian, F. Q. Nie, Y. Zhao, J. Zhai and L. Jiang, *Nature*, 2010, **463**, 640.
2 X. Gao, X. Yan, X. Yao, L. Xu, K. Zhang, J. Zhang, B. Yang and L. Jiang, *Adv. Mater.*, 2007, **19**, 2213.
3 X. Gao and L. Jiang, *Nature*, 2004, **432**, 36.
4 (*a*) W. Barthlott and C. Neinhuis, *Planta*, 1997, **202**, 1; (*b*) S. Herminghaus, *Europhys. Lett.*, 2000, **52**, 165.
5 (*a*) R. N. Wenzel, *Ind. Eng. Chem.*, 1936, **28**, 988; (*b*) A. B. D. Cassie and S. Baxter, *Trans. Faraday Soc.*, 1944, **40**, 546; (*c*) M. Callies and D. Quéré, *Soft Matter*, 2005, **1**, 55; (*d*) A. Marmur, *Langmuir*, 2003, **19**, 8343; (*e*) M. Nosonovsky, *Langmuir*, 2007, **23**, 3157; (*f*) D. Öner and T. J. McCarthy, *Langmuir*, 2000, **16**, 7777.
6 (*a*) R. Blossey, *Nat. Mater.*, 2003, **2**, 301; (*b*) Q. Xie, J. Xu, L. Fen, L. Jiang, W. Tang, X. Luo and C. C. Han, *Adv. Mater.*, 2004, **16**, 302; (*c*) N. J. Shirtcliffe, G. McHale, M. I. Newton, G. Chabrol and C. C. Perry, *Adv. Mater.*, 2004, **16**, 1929; (*d*) F. Shi, Z. Q. Wang and X. Zhang, *Adv. Mater.*, 2005, **17**, 1005; (*e*) A. Nakajima, K. Hashimoto and T. Watanabe, *Monatsh. Chem.*, 2001, **132**, 31; (*f*) D. Quéré, *Rep. Prog. Phys.*, 2005, **68**, 2495.
7 (*a*) M. Liu, S. Wang, Z. Wei, Y. Song and L. Jiang, *Adv. Mater.*, 2009, **21**, 665; (*b*) W. Barthlott, T. Schimmel, S. Wiersch, K. Koch, M. Brede, M. Barczewski, S. Walheim, A. Weis, A. Kaltenmaier, A. Leder and H. F. Bohn, *Adv. Mater.*, 2010, **22**, 2325.
8 X. Zhang, F. Shi, J. Niu, Y. G. Jiang and Z. Q. Wang, *J. Mater. Chem.*, 2008, **18**, 621.
9 (*a*) D. W. Fuerstenau and R. Herrera-Urbina, *Surfactant Sci. Ser.*, 1989, **33**, 259; (*b*) H. Odegaard, *Water Sci. Technol.*, 2001, **43**, 75; (*c*) J. Drelich and J. D. Miller, *Prog. Paper Recyc.*, 2001, **11**, 38.
10 J. Wang, Y. Zheng, F. Q. Nie, J. Zhai and L. Jiang, *Langmuir*, 2009, **25**, 14129.
11 L. Feng, Y. Zhang, J. Xi, Y. Zhu, N. Wang, F. Xia and L. Jiang, *Langmuir*, 2008, **24**, 4114.
12 M. Wang, Q. Yang, C. Wang, J. Wang and L. Jiang, *Chem. J. Chinese Universities*, 2011, **32**, 1594.
13 B. Bhushan and E. K. Her, *Langmuir*, 2010, **26**, 8207.
14 (*a*) C. M. Phan, A. V. Nguyen and G. M. Evans, *J. Colloid Interface Sci.*, 2006, **296**, 669; (*b*) A. Beaussart, L. Parkinson, A. Mierczynska-Vasilev, J. Ralston and D. A. Beattie, *Langmuir*, 2009, **25**, 13290.
15 A. S. Najafi, Z. Xu and J. Masliyah, *Can. J. Chem. Eng.*, 2008, **86**, 1001.
16 M. Jin, X. Feng, L. Feng, T. Sun, J. Zhai, T. Li and L. Jiang, *Adv. Mater.*, 2005, **17**, 1977.
17 (*a*) Z. Guo, W. Liu and B. Su, *Appl. Phys. Lett.*, 2008, **92**, 063104; (*b*) I. Mohammed-Ziegler, Á. Oszlánczi, B. Somfai, Z. Hórvöloyi, I. Pászli, A. Holmgren, W. Forsling and J. Adhesion, *Sci. Technol*, 2004, **18**, 687; (*c*) M. Nosonovsky and B. Bhushan, *J. Phys.: Condens. Matter*, 2008, **20**, 225009.
18 X. Yao, Q. Chen, L. Xu, Q. Li, Y. Song, X. Gao, D. Quéré and L. Jiang, *Adv. Funct. Mater.*, 2010, **20**, 656.
19 (*a*) J. A. Rogers, T. Someya and Y. Huang, *Science*, 2010, **327**, 1603; (*b*) P. Lin and S. Yang, *Appl. Phys. Lett.*, 2007, **90**, 241903.
20 P. G. de Gennes, F. Brochard-Wyart, D. Quéré, *Capillarity and We tting Phenomena-Drops, Bubbles, Pearls, Waves*, Springer, New York, USA 2002, Ch. 9.

